Article

Cell Reports

HAND2 Target Gene Regulatory Networks Control Atrioventricular Canal and Cardiac Valve Development

Graphical Abstract

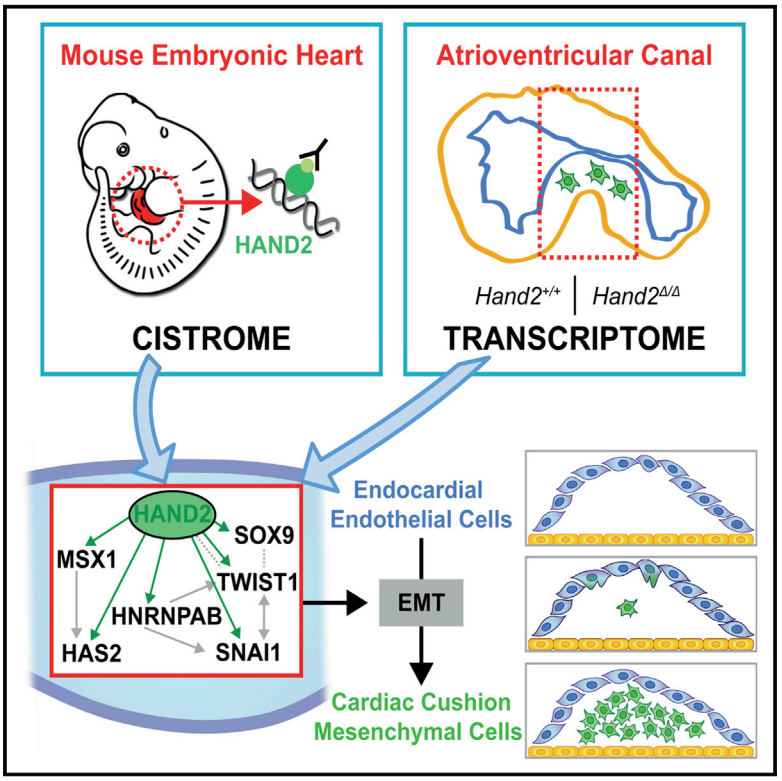

Authors

Frédéric Laurent, Ausra Girdziusaite, Julie Gamart, ..., Axel Visel, Aimée Zuniga, Rolf Zeller

Correspondence

rolf.zeller@unibas.ch

In Brief

Laurent et al. combine ChIP-seq with transcriptome analysis to identify the HAND2 target gene network that controls the EMT and mesenchymal cell migration during cardiac cushion formation in the atrioventricular canal (AVC). The HAND2 transcriptional targets include *Snai1*, whose re-expression in *Hand2*-deficient AVC explants partially restores mesenchymal cell migration.

Highlights

- HAND2 controls development of the AVC cardiac cushions forming mitral/tricuspid valves
- HAND2 is a key regulator of the EMT underlying cardiac cushion mesenchyme formation
- Identification of the HAND2 target gene networks that control EMT and AVC development
- HAND2 acts upstream of the EMT key regulator *Snai1* in AVC and other embryonic tissues

Accession Numbers

GSE73368
GSE94246

Laurent et al., 2017, Cell Reports *19*, 1602–1613
May 23, 2017
http://dx.doi.org/10.1016/j.celrep.2017.05.004

OPEN ACCESS
CellPress

Cell Reports
Article

HAND2 Target Gene Regulatory Networks Control Atrioventricular Canal and Cardiac Valve Development

Frédéric Laurent,[1,7] Ausra Girdziusaite,[1,7] Julie Gamart,[1] Iros Barozzi,[2] Marco Osterwalder,[1,2] Jennifer A. Akiyama,[2] Joy Lincoln,[3] Javier Lopez-Rios,[4] Axel Visel,[2,5,6] Aimée Zuniga,[1,8] and Rolf Zeller[1,8,9,*]

[1]Developmental Genetics, Department of Biomedicine, University of Basel, 4058 Basel, Switzerland
[2]Functional Genomics Department, Lawrence Berkeley National Laboratory, Berkeley, CA 94720, USA
[3]Center for Cardiovascular and Pulmonary Research, The Research Institute at Nationwide Children's Hospital, Columbus, OH 43205, USA
[4]Development and Evolution, Department of Biomedicine, University of Basel, 4058 Basel, Switzerland
[5]U.S. Department of Energy Joint Genome Institute, Walnut Creek, CA 94598, USA
[6]School of Natural Sciences, University of California, Merced, CA 95343, USA
[7]These authors contributed equally
[8]Senior author
[9]Lead Contact
*Correspondence: rolf.zeller@unibas.ch
http://dx.doi.org/10.1016/j.celrep.2017.05.004

SUMMARY

The HAND2 transcriptional regulator controls cardiac development, and we uncover additional essential functions in the endothelial to mesenchymal transition (EMT) underlying cardiac cushion development in the atrioventricular canal (AVC). In *Hand2*-deficient mouse embryos, the EMT underlying AVC cardiac cushion formation is disrupted, and we combined ChIP-seq of embryonic hearts with transcriptome analysis of wild-type and mutants AVCs to identify the functionally relevant HAND2 target genes. The HAND2 target gene regulatory network (GRN) includes most genes with known functions in EMT processes and AVC cardiac cushion formation. One of these is *Snai1*, an EMT master regulator whose expression is lost from *Hand2*-deficient AVCs. Re-expression of *Snai1* in mutant AVC explants partially restores this EMT and mesenchymal cell migration. Furthermore, the HAND2-interacting enhancers in the *Snai1* genomic landscape are active in embryonic hearts and other *Snai1*-expressing tissues. These results show that HAND2 directly regulates the molecular cascades initiating AVC cardiac valve development.

INTRODUCTION

Perturbations affecting cardiac progenitors result in embryonic lethality and severe congenital heart defects, which are a major cause of infant and even adult mortality (Bruneau, 2008). In particular, different types of congenital heart defects are caused by alterations in the progenitors of the second heart field (SHF; reviewed by Kelly, 2012). SHF progenitors migrate into the developing heart tube, where they contribute to most developing structures including the inflow pole, both atria and ventricles, and the outflow tract (OFT). The four heart chambers are formed by rapid proliferative expansion, while the cardiomyocytes in the OFT and atrioventricular canal (AVC) proliferate less and remain undifferentiated (Christoffels et al., 2010; Greulich et al., 2011). The AVC connects the left ventricle to the forming atria, is required for chamber septation, and gives rise to the atrioventricular node and mitral and tricuspid valves (Christoffels et al., 2010; Lin et al., 2012). In mouse embryos, development of the AVC valves begins at embryonic day E9.5, when endocardial cells undergo an endothelial to mesenchymal transition (EndMT or EMT) in response to signals from the myocardium. The delaminating endocardial cells migrate into the cardiac jelly and give rise to the cardiac cushion mesenchyme, which are then remodeled into the mature valve structures (MacGrogan et al., 2014). The EMT in the AVC is controlled by BMP2 signaling from the myocardium, which synergizes with myocardial TGFβ2 and endocardial NOTCH signaling to activate downstream effectors that include the *Snai1* transcriptional regulator (Luna-Zurita et al., 2010; Ma et al., 2005; Niessen et al., 2008; Timmerman et al., 2004). SNAI1 is a key EMT regulator in embryos and various diseases such as tumor metastasis (reviewed by Nieto, 2011). Its inactivation in the endothelial compartment disrupts the EMT underlying AVC cardiac cushion formation (Wu et al., 2014).

Another transcription factor essential for heart development is HAND2, which also functions in developing branchial arches and limb buds (Srivastava et al., 1997). In the developing heart, HAND2 is expressed in the myocardial compartment of the right ventricle and OFT, the epicardium, and valve progenitors in both OFT and AVC (VanDusen and Firulli, 2012; VanDusen et al., 2014b). Consistent with its complex expression pattern, genetic inactivation of *Hand2* in mice disrupts development of limb buds, branchial arches, aortic arch arteries, and the right ventricle, which causes embryonic lethality (Srivastava et al., 1997).

Specific inactivation in developing heart tissues has revealed essential *Hand2* functions in the cardiac neural crest cells that contribute to cardiac cushions in the OFT, survival of SHF progenitors, heart chamber trabeculation, and epicardial cell differentiation (Barnes et al., 2011; Holler et al., 2010; Tsuchihashi et al., 2011; VanDusen et al., 2014a). Previous studies had also pointed to HAND2 functions in cardiac cushion formation, but the potential essential functions have not been identified (Holler et al., 2010; Liu et al., 2009; VanDusen et al., 2014a). In humans, mutations in *HAND2* have been linked to congenital heart malformations that include ventricular septal defects (Shen et al., 2010; Sun et al., 2016).

We have used chromatin immunoprecipitation sequencing (ChIP-seq) to define the genome-wide interaction profile of endogenous HAND2 chromatin complexes in mouse embryonic hearts. This analysis shows that HAND2 interacts with non-coding regions associated with a large number of genes functioning during heart development. Most importantly, our analysis revealed essential HAND2 functions in the EMT underlying AVC cardiac cushion formation, which is disrupted in *Hand2*-deficient embryos. Combining transcriptome analysis of wild-type and *Hand2*-deficient AVCs with the HAND2 ChIP-seq dataset identified the HAND2 target genes that function in AVC cardiac cushion development. In particular, this analysis revealed that the EMT regulator *Snai1* is a transcriptional target of HAND2. The failure of endocardial cells to invade the cardiac jelly in *Hand2*-deficient AVCs is partially restored by re-expressing SNAI1 in mutant explants. Last but not least, we show that the two *Snai1*-associated enhancers interacting with HAND2 chromatin complexes recapitulate major aspects of *Snai1* expression in mouse embryos.

RESULTS

Genomic Regions Enriched in Endogenous HAND2 Chromatin Complexes Identify the Range of HAND2 Target Genes in Mouse Embryonic Hearts

The *Hand2*^{3xF} allele, which encodes a HAND2 protein with a 3xFLAG epitope tag inserted in its N-terminal part (Osterwalder et al., 2014), was used to profile the genomic regions enriched in HAND2-chromatin complexes. Anti-FLAG antibodies were used for chromatin immunoprecipitation, which was followed by massive parallel sequencing (ChIP-seq). To obtain sufficient chromatin for ChIP-seq, ~300 hearts per biological replicate were dissected from *Hand2*$^{3xF/3xF}$ mouse embryos at embryonic days E10.25–10.5. Two biological replicates were analyzed, and the genome-wide binding profiles using model-based analysis of ChIP-seq (MACS) (Zhang et al., 2008) identified 12,117 significantly enriched genomic regions. Genomic Regions Enrichment of Annotations Tool (GREAT) analysis (McLean et al., 2010) was used to assign these 12,117 regions to 7,792 neighboring genes, which defines the initial set of putative HAND2 targets (Table S1; Supplemental Experimental Procedures). Most of the genomic regions enriched in HAND2 chromatin complexes are located ≥10 kb away from transcriptional start sites (TSS) and encode evolutionary conserved sequences that overlap the peak summit (Figures 1A and 1B). Functional enrichment was assessed by GREAT using increasingly larger set of peaks (pool of incremental deciles; for details, see Supplemental Experimental Procedures). This analysis revealed that terms related to abnormal cardiac morphology and heart development were already enriched when using only the most enriched regions, while terms referring to specific processes such as OFT, right ventricle, and AVC development reached significance using the larger dataset (Figure S1A). In particular, 15 of the 16 most enriched Gene Ontology (GO) terms are relevant to heart development, while the remaining term identifies genes functioning in EMT processes (Figure 1C, see below). De novo motif discovery using HOMER (Heinz et al., 2010) identified the consensus *Ebox* motif (CATCTG; Dai and Cserjesi, 2002) as the most prevalent among HAND2 peaks (Figure 1D). Other significantly enriched motifs include binding sites for GATA transcription factors (Figure S1B), which are key regulators of heart development (Stefanovic and Christoffels, 2015). Indeed, computational comparison of the HAND2 (Table S1) with a published GATA4 ChIP-seq dataset (using whole mouse embryonic hearts at E12.5; He et al., 2014) shows that 28.3% of the enriched genomic regions are shared between the two datasets, which is 15-fold higher than expected by chance (data not shown). As development of *Hand2*-deficient mouse embryos results in lethality by ~E10.5 (Srivastava et al., 1997), we limited our analysis to mutant embryos at E9.0–9.5. During this early organogenic stage, no aberrant apoptosis occurs in the developing heart in contrast to branchial arches and frontonasal mass (Figure S1C). Therefore, all interactions of HAND2 chromatin complexes with candidate *cis*-regulatory modules (CRMs) associated with genes of interest were also verified by ChIP-qPCR using embryonic hearts at E9.25–9.5 (Figures 1, 4, S3, and S6).

To validate the ChIP-seq dataset as a resource for identifying HAND2 target genes, we determined which of the genes with known alterations in their expression are associated with HAND2 ChIP-seq peaks (Table S2 and references therein). This analysis showed that about half of these genes are associated with at least one HAND2 ChIP-seq peak (n = 56/114; Table S2, see also Table S1). This suggests that their altered expression in *Hand2*-deficient hearts could be a consequence of direct transcription regulation by HAND2. Next, we overlapped the HAND2 binding profiles with enhancers active in mouse embryonic hearts that were identified by a large enhancer screen (VISTA Enhancer Browser: https://enhancer.lbl.gov, Visel et al., 2007). This analysis showed that 71 of the 193 VISTA enhancers active in mouse embryonic hearts overlap with HAND2 ChIP-seq peaks (Figures 1E, 1F, and S2; Table S3). These enhancers include CRMs in the genomic landscapes of the *Gata4*, *Gata6*, *Myocd*, and *Tbx20* transcriptional regulators, which are essential for OFT and/or right ventricle development. Whole-mount in situ hybridization (WISH) showed that the expression of *Gata4*, *Myocd*, and *Gata6* is reduced in *Hand2*-deficient hearts, while the expression of *Tbx20* appears unchanged (E9.25–9.5, Figure 1G). The requirement of *Hand2* for OFT and right ventricle development is also supported by GO analysis as more than half of the genes with annotated functions in OFT and right ventricle (RV) development are associated with HAND2 ChIP-seq peaks (Figure S3A; Table S4). In particular, several ligands of the signaling pathways required for development of these structures are identified as HAND2 target genes (Figures S3B

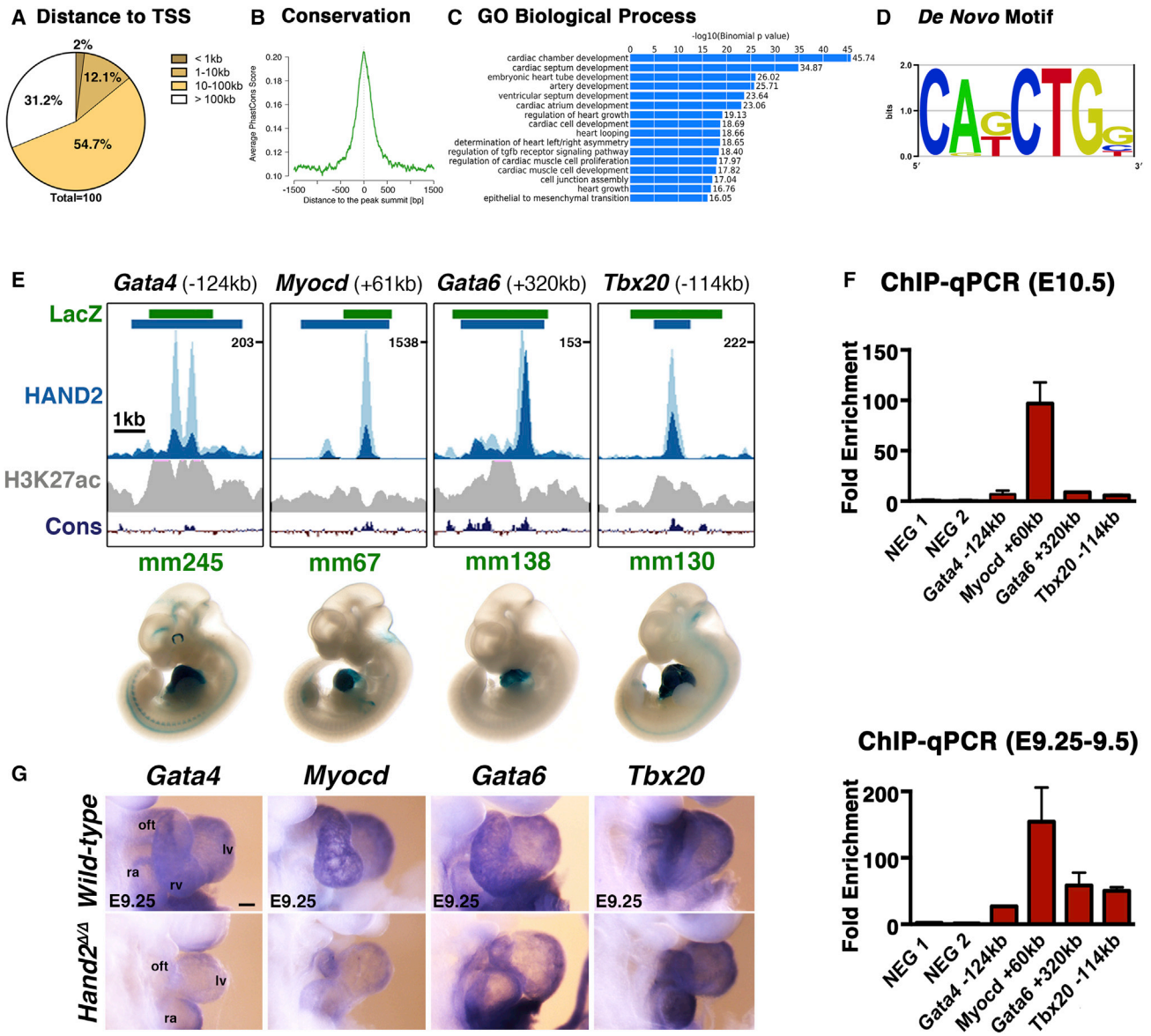

Figure 1. ChIP-Seq Analysis Using the *Hand2*^{3xF} Allele Identifies the HAND2 Cistrome in Mouse Embryonic Hearts

(A) The majority of the genomic regions enriched in HAND2 chromatin complexes from mouse embryonic hearts at E10.5 map ≥10 kb away from the closest transcription start site (TSS).

(B) In addition, the majority of the HAND2-interacting genomic regions are evolutionarily conserved.

(C) The top GO terms associated with HAND2 candidate targets reveal the preferential enrichment of genes functioning in cardiac development.

(D) The consensus *Ebox* motif is most enriched by de novo motif discovery.

(E) Selection of VISTA enhancers enriched in HAND2 chromatin complexes. Green intervals indicate the regions with enhancer activity (VISTA enhancer database); blue intervals highlight the regions enriched in HAND2 chromatin complexes (MACS peaks). Distances to the nearest TSS within the TAD are indicated on top. ChIP-seq profiles of the two biological replicates (E10.5) are shown in light and dark blue, respectively. The H3K27ac ChIP-seq profile for mouse hearts (E11.5) is shown in gray (Nord et al., 2013). The scheme at the bottom shows the placental mammal conservation (Cons) plot (PhyloP). Representative transgenic *LacZ* reporter embryos for VISTA enhancers associated with genes functioning in OFT and/or right ventricle development (*Gata4*, *Myocd*, *Gata6*, and *Tbx20*) are shown below.

(F) ChIP-qPCR validation of the ChIP-seq peaks (E) for mouse embryonic hearts at E10.5 (n = 3 biological replicates) and E9.25 (n = 2; mean ± SD).

(G) Expression of the HAND2 targets *Gata4*, *Myocd*, *Gata6*, and *Tbx20* in wild-type and *Hand2*-deficient (*Hand2*$^{\Delta/\Delta}$) embryonic hearts (E9.25).

Scale bars, 100 μm. oft, outflow tract; ra, right atrium; rv, right ventricle; lv, left ventricle; avc, atrioventricular canal; la, left atrium. See also Figures S1–S3 and Tables S1 and S2–S4.

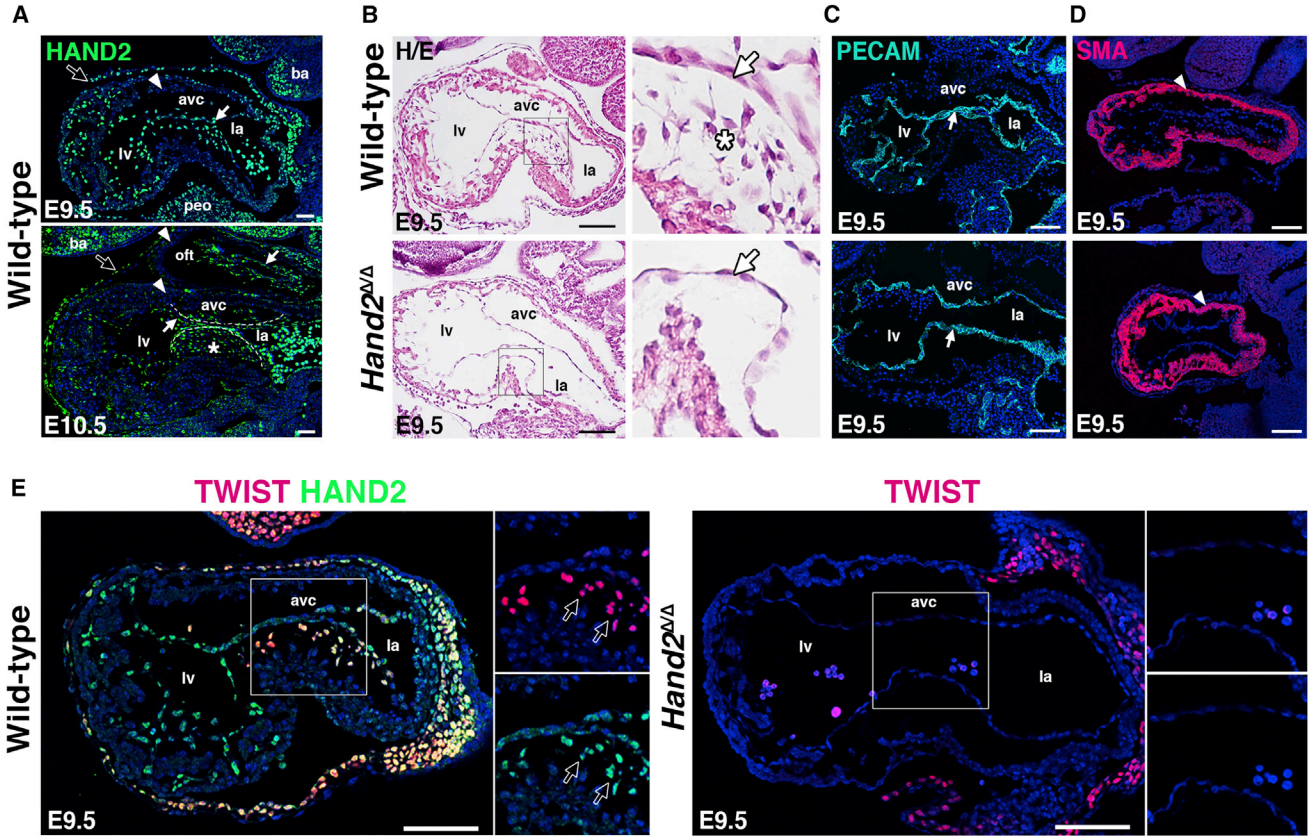

Figure 2. AVC Cardiac Cushion Agenesis in *Hand2*-Deficient Mouse Embryos

(A) Distribution of the endogenous HAND2^{3xF} protein (using anti-FLAG antibodies, green fluorescence) during in mouse embryonic hearts at E9.5 and E10.5. Representative sagittal sections are shown. White arrows, endocardium; white arrowheads, myocardium; white asterisks, HAND2 expressing AVC cardiac cushion mesenchymal cells; black arrows, epicardium. Scale bars, 50 μm.

(B) H&E staining reveals the absence of delaminating endocardial cells with mesenchymal characteristics (white asterisks) in the AVC of *Hand2*-deficient mouse embryos. White arrow, endocardium. Scale bars, 100 μm.

(C) Detection of the platelet endothelial cell adhesion molecule (PECAM) in the endocardium of wild-type and *Hand2*-deficient embryos (white arrow).

(D) Detection of smooth muscle actin (SMA) in the AVC myocardium of wild-type and *Hand2*-deficient embryos (white arrowhead). Myocardium (A–D).

(E) Colocalization of the HAND2^{3xF} (green fluorescence) with TWIST1 transcriptional regulators (red fluorescence) in the AVC of wild-type (*Hand2*$^{3xF/3xF}$) and *Hand2*-deficient (*Hand2*$^{\Delta/\Delta}$) embryos at E9.5. Colocalization is detected in delaminating mesenchymal cells (indicated by arrows, left panel), which are missing from the mutant AVC (right panel).

Scale bars in panels (E) AND (F), 100 μm. avc, atrioventricular canal; ba, branchial arches; la, left atrium; lv, left ventricle; oft, outflow tract; peo, proepicardial organ.

and S3C). This includes *Wnt11*, *Wnt5a*, *Bmp4*, *Tgfβ2*, and *Fgf10*, whose expression is either reduced or lost from the OFT and/or RV of *Hand2*-deficient mouse embryos (E8.75–9.25, Figure S3C). Collectively, this first analysis shows that a significant fraction of genes functioning in mouse OFT and RV morphogenesis are likely HAND2 target genes (Figures 1G and S3). However, not all candidate target genes analyzed are altered in *Hand2*-deficient hearts, which points either to *cis*-regulatory redundancy or raises the possibility that the interaction of HAND2 complexes with the candidate CRMs is not essential for the adjacent genes.

HAND2 Is a Key Regulator of the EMT during AVC Cardiac Cushion Formation

Strikingly, the GO analysis identified EMT as one of the key biological processes associated with the HAND2 cistrome (Figure 1C). An essential process during heart valve development is formation of the mesenchymal compartment of the AVC cardiac cushions as endocardial cells undergo an EMT (see Introduction). In wild-type hearts, HAND2 proteins are expressed by endocardial cells in the AVC, the cells undergoing EMT and the delaminating cells forming the cushion mesenchyme continue to express HAND2 (asterisk, Figure 2A and data not shown). Furthermore, histological analysis reveals the complete absence of mesenchymal cells in the AVC cardiac cushions of *Hand2*-deficient hearts at E9.0–9.5, which points to disruption of the EMT process (Figure 2B). As the distribution of platelet endothelial cell adhesion molecule (PECAM) and smooth muscle actin (SMA) positive cells is not altered in *Hand2*-deficient hearts, the endocardial and myocardial compartments of the AVC appear to have formed normally, which underscores the specific nature of the observed cellular defect

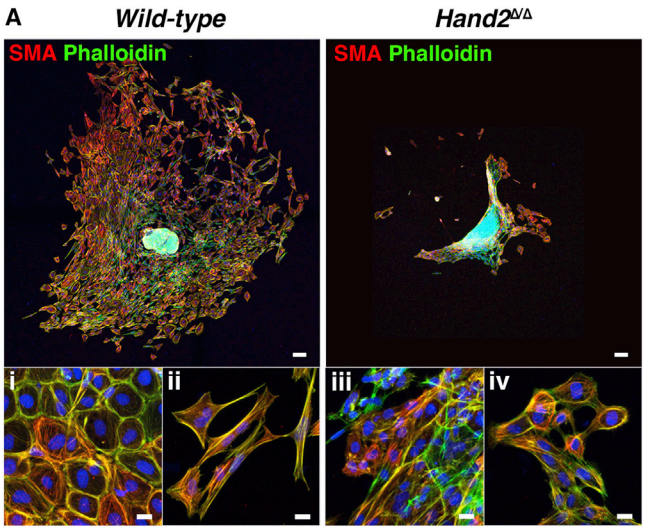

Figure 3. *Hand2*-Deficient AVC Endocardial Cells Fail to Initiate EMT and Mesenchymal Cell Migration

(A) Smooth muscle actin (red) and F-actin (green Phalloidin staining) distribution in cells that have migrated into the matrix from AVC explants of wild-type and *Hand2*-deficient embryos after 72 hr in culture. Scale bars, 100 μm. Bottom panels show cells in proximity to the explant (i and iii) and at the far edge of migration (ii and iv). Scale bars, 20 μm. (B) Quantification of the numbers of cells that migrated into the matrix from wild-type (n = 10) and *Hand2*-deficient AVC explants (n = 7). The mean ± SD (p = 0.0001, Mann-Whitney test) and all individual data points are shown.

(Figures 2C and 2D). TWIST1 forms hetero-dimeric transcriptional complexes with HAND2 and regulates cardiac cushion development (Firulli et al., 2005; VanDusen and Firulli, 2012). Therefore, the distribution of both proteins was comparatively analyzed in developing AVC cardiac cushions (Figure 2E). In wild-type embryos, HAND2 and TWIST1 are co-expressed by the delaminating mesenchymal cells that form the AVC cardiac cushions in wild-type hearts (left panels, Figure 2E). In contrast, these TWIST1-positive cells are absent in *Hand2*-deficient hearts (right panel, Figure 2E). Together, these results point to complete disruption of AVC cardiac cushion formation in *Hand2*-deficient mouse embryos.

To study this processes further, AVCs were dissected from wild-type and mutant hearts at E9.5 and cultured on collagen matrices for 72 hr (Figure 3A, Camenisch et al., 2000). Then, the mesenchymal cells that had migrated from the explant into the matrix were quantitated (Figure 3B): on average 330 ± 40 cells colonize the matrix in wild-type AVC explants (n = 10), while ~10-fold fewer mesenchymal cells (36 ± 3) are detected in AVC explants isolated from *Hand2*-deficient embryos (n = 7). In particular, wild-type endocardial cells in proximity of the AVC explant retain their cobblestone-like morphology and a cortical actin ring (Figure 3A, i), while cells that migrated further develop actin stress fibers and long filopodia characteristic of mesenchymal cells (Figure 3A, ii). In contrast, the few cells invading the matrix in cultures of *Hand2*-deficient AVCs mostly retain their cobblestone-like morphology (Figure 3A, iii and iv). This loss of mesenchymal characteristics shows that the endocardial cells of *Hand2*-deficient AVCs fail to undergo the EMT giving rise to the mesenchymal cell forming the cardiac cushions.

HAND2 Controls the Expression of Genes that Function in the EMT Underlying AVC Cardiac Cushion Formation

To identify the gene regulatory networks (GRNs) controlled by HAND2 during AVC cardiac cushion formation, the transcriptomes of dissected wild-type and *Hand2*-deficient AVCs were analyzed (E9.0–9.25: 18–23 somites; see Supplemental Experimental Procedures). Statistical analysis showed that 1,051 genes are differentially expressed (DEGs: 695 are upregulated and 365 downregulated, Figure 4A; Table S5; Figure S4A for GO analysis). Among these genes, the transcriptional targets of HAND2 were identified as those genes harboring one or more HAND2 ChIP-seq peaks in their topologically associating domains (TADs, Dixon et al., 2012; Figures 4B, 4C, and S4B; Table S5). This analysis shows that the TADS of DEGs contain on average a significantly larger number of HAND2-interacting regions (median ~5) than genes whose expression is not altered (median ~1; Figure 4B). GO analysis of these HAND2 transcriptional targets indicates that the 167 DEGs, whose expression is downregulated in *Hand2*-deficient AVCs function preferentially in heart and organ development (including cardiac EMT and mesenchyme development), while the 372 upregulated DEGs function preferentially in cardiovascular and blood vessel development (Figure 4C). In particular, this functional annotation identified a subset of 24 DEGs that function in EMT processes and/or AVC cushion formation (Figure S4C). Combining the transcriptome analysis with HAND2 ChIP-qPCR analysis establishes 19 of these DEGs as direct transcriptional targets of HAND2 in developing hearts at E9.25–9.5 (Figures 4D and 4E). Transcriptome analysis showed that the expression of seven of these HAND2 targets is downregulated, while 12 are upregulated in mutant AVCs (Figure 4D; Table S6). These differential effects are not unexpected as HAND2 transcriptional complexes are known to differentially activate or repress gene expression (see Discussion). Together, this analysis uncovers the HAND2 target GRN functioning in AVC cardiac cushion formation and reveals the differential effects of the *Hand2* deficiency on gene expression in the mutant AVC (Figures 4D and 4E).

Next, we used WISH to detect spatial alterations in the AVC of *Hand2*-deficient hearts at E9.25–9.5 (Figures 5 and S5). To uncover potential global molecular changes in the mutant AVC, we first analyzed the spatial distribution of key regulators whose transcript levels are not changed (*Bmp2*, *Hey2*, *Notch1*, *Rbpj*, *Snai2*, *Epha3*, *Tbx20*; Figures 5A and 5B; Table S5 and data not shown). The spatial distribution of all of these genes is comparable to wild-types in mutant AVCs, as exemplified by the EMT-inducer *Bmp2* and the NOTCH transcriptional target *Hey2* (Figures 5A and 5B). This indicates that the AVC domain

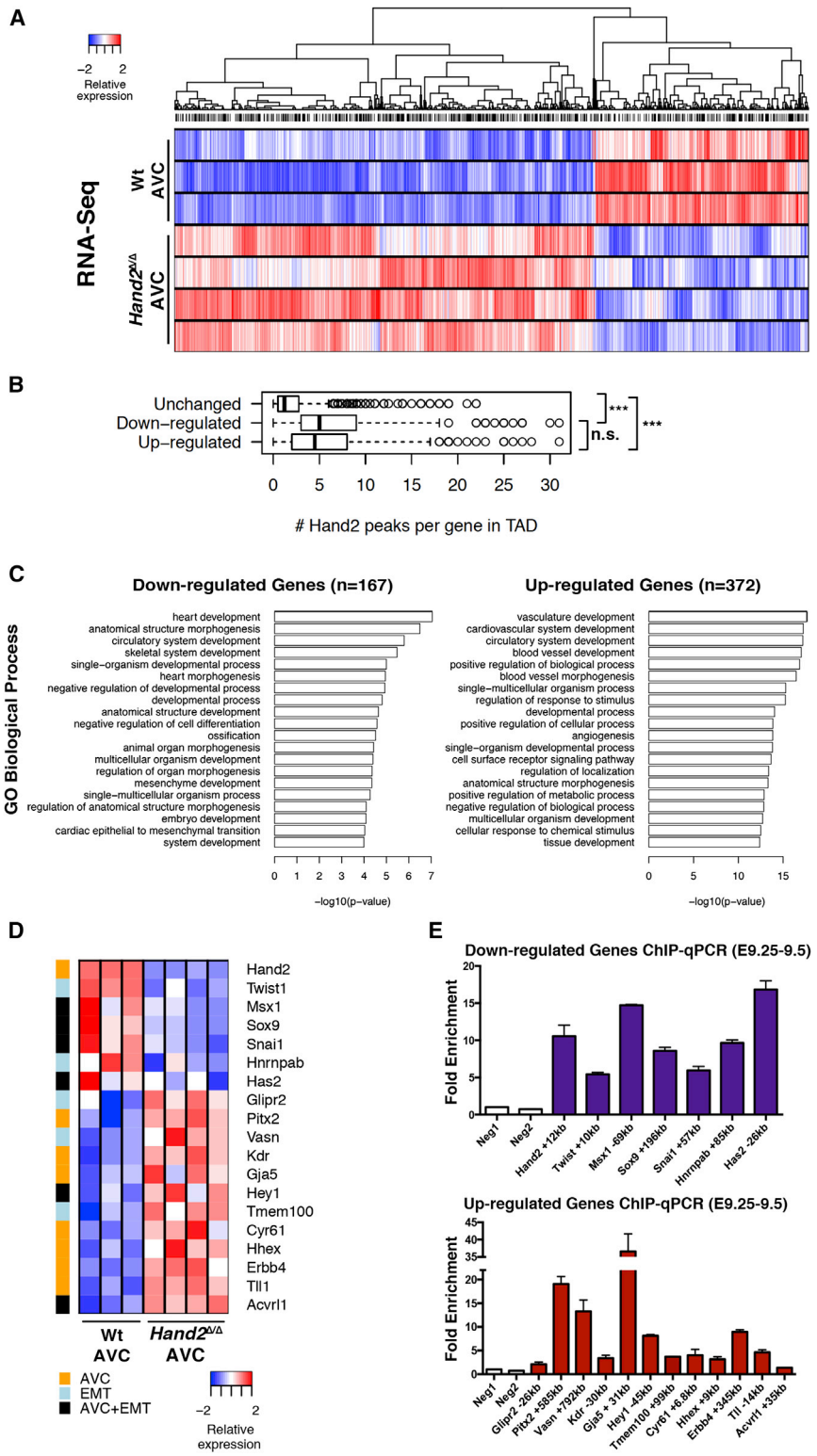

Figure 4. Transcriptome Analysis Identifies the Transcriptional Targets of HAND2 in the AVC

(A) Heatmap of the differentially expressed genes (DEGs) identified by comparing the transcriptomes of wild-type and *Hand2*-deficient AVCs from mouse embryonic hearts at E9.25–9.5 (n = 4 and n = 3 biological replicates were analyzed for mutant and wild-type AVCs, respectively). DEGs are genes whose expression is significantly changed (≥1.5-fold) between wild-type and mutant samples ($p < 0.05$).

(B) The boxplot shows the number of HAND2 ChIP-seq peaks in the TADs harboring genes with unchanged, down- or upregulated expression in mutant AVCs, respectively. The TADs of genes with altered expression encode more HAND2-interacting genomic regions. To account for the different numbers of genes and HAND2 ChIP-seq peaks per TAD, peak counts were normalized as numbers of peaks per gene for each TAD.

(C) GO enrichment analysis for biological processes for the 167 downregulated and 372 upregulated genes (in mutant AVCs) that contain HAND2 ChIP-seq peaks in their TADs.

(D) GO analysis to identify the HAND2 target genes with annotated functions in EMT processes and AV cushion morphogenesis.

(E) Mouse embryonic hearts isolated at E9.25–9.5 were used for ChIP-qPCR validation of the most prominent HAND2 ChIP-seq peaks in the TADs of the genes shown in D (n = 4 using two biological replicates, mean ± SD, $p \leq 0.05$). See also Figure S4 and Tables S5 and S6.

is correctly specified in mutant hearts and corroborates the specificity of the molecular alterations underlying the cardiac cushion agenesis (Figures 2 and 3). WISH analysis of HAND2 target genes with significantly changed transcript levels (Figure 4D; Table S6) failed to detect spatial alterations for several of them due to low and/or uniform expression (low: *Vasn*, *Tmem100*, *Erbb4*, *Tll1*, and *Acvrl*, uniform: *Cyr61* and *Hnrnapab*, data not shown). Furthermore, the small but significant differences in transcript levels for several additional DEGs could not be reliably detected by WISH (*Pitx2*, *Glipr2*, *Kdr*, *Gja5*, Figure S5A and data not shown), likely due to the qualitative nature of in situ hybridization that best detects spatial changes. This is exemplified by the fact that WISH revealed the ectopic expression of two transcriptionally upregulated HAND2 target genes in mutant AVCs, namely, the NOTCH1 transcriptional mediator *Hey1* and the homeobox transcription factor *Hhex* (Figures 5C and 5D).

In agreement with the reduced expression detected by RNA-seq (Figure 4D; Table S6), WISH corroborates the loss of the transcriptional regulators *Twist1* (Figure 5E, see also Figure 2E),

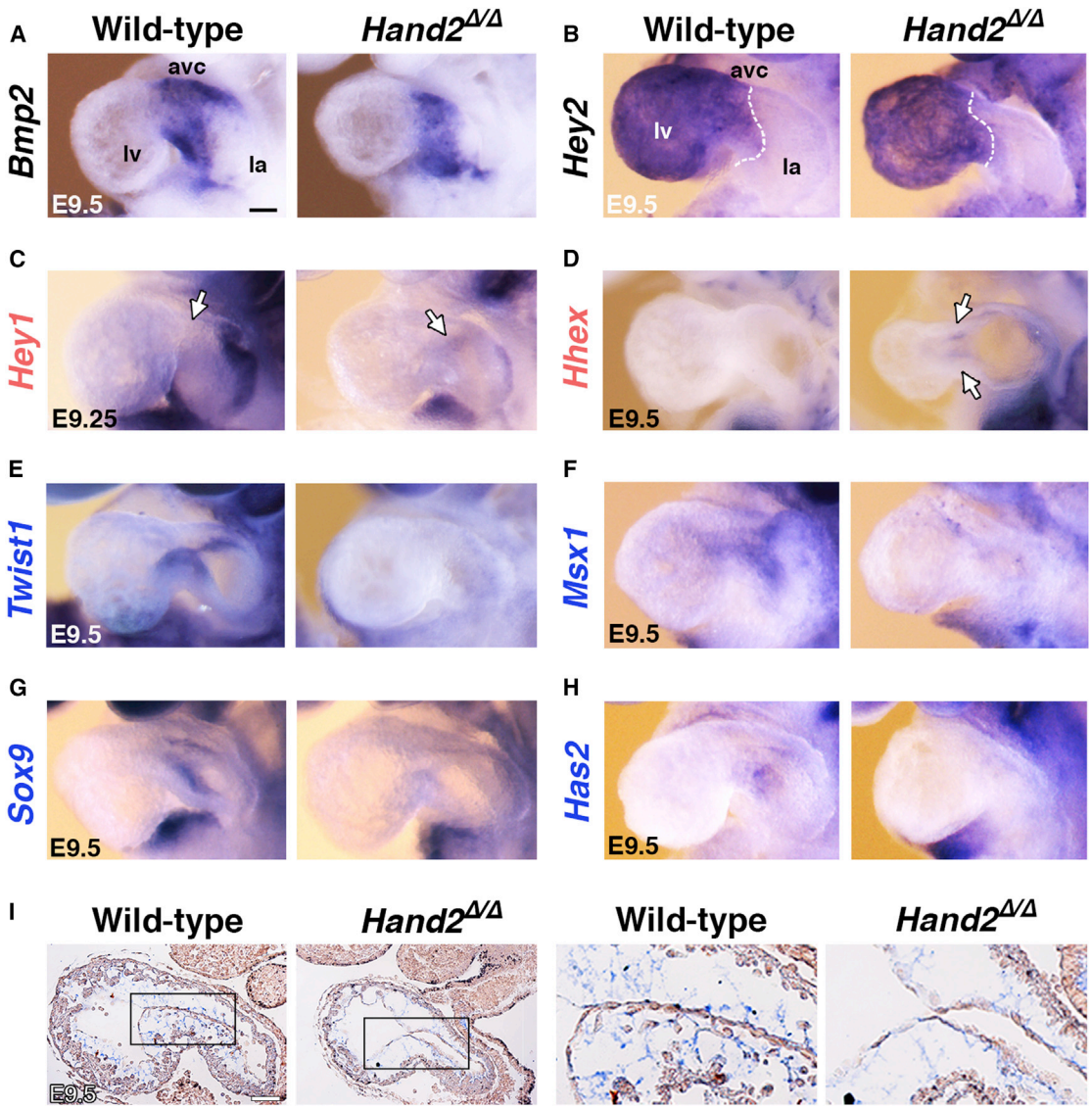

Figure 5. Whole-Mount in Situ Hybridization Reveals Spatial Changes in Some of the Differentially Expressed HAND2 Target Genes

(A and B) Unaltered expression of *Bmp2* (A) and *Hey2* (B) indicates that the AVC domain is established correctly in *Hand2*-deficient hearts.

(C and D) Ectopic expression of the *Hey1* (C) and *Hhex* transcriptional regulators (D) in the mutant AVC corroborated their upregulation detected by RNA-seq analysis.

(E–H) Loss of *Twist1* (E), *Msx1* (F), Sox9 (G), and *Has2* (H) from the mutant AVC is in agreement with their transcriptional downregulation detected by RNA-seq analysis.

(I) Alcian blue staining of glycosaminoglycans shows the reduced deposition of extra-cellular matrix in the cardiac jelly of *Hand2*-deficient mouse embryos. Right panels show the enlargements indicated by frames in the left panels. Gene names in black, unaltered; red, increased; blue, reduced transcript levels as determined by RNA-seq analysis (Figure 4).

Scale bars, 100 μm. See also Figure S5.

Msx1 (Figure 5F), and *Sox9* (Figures 5G and S5B) from mutant AVCs by E9.5. The downregulation of *Msx1* indicates that BMP signal transduction is disrupted in the mutant AVC (Figure 5F; Table S6). SOX9 regulates the proliferation of the mesenchymal progenitor cells, and its loss agrees with the lack of delaminating mesenchymal cells in mutant AVCs (Figures 5G and S5B; Akiyama et al., 2004). Most relevant to the disrupted EMT (Figure 3), the expression of *Has2* and *Snai1* is significantly downregulated in *Hand2*-deficient AVCs (Figure 4D). *Has2* encodes the enzyme that produces hyaluronic acid in the cardiac jelly (Camenisch et al., 2000). Genetic inactivation of the mouse *Has2* gene disrupts both cardiac jelly deposition and mesenchymal cell migration during cardiac cushion development. In *Hand2*-deficient hearts, the loss of *Has2* is paralleled by reduced extra-cellular matrix/cardiac jelly deposition (Figures 5H and 5I). Camenisch et al. (2000) showed that treatment of *Has2*-deficient

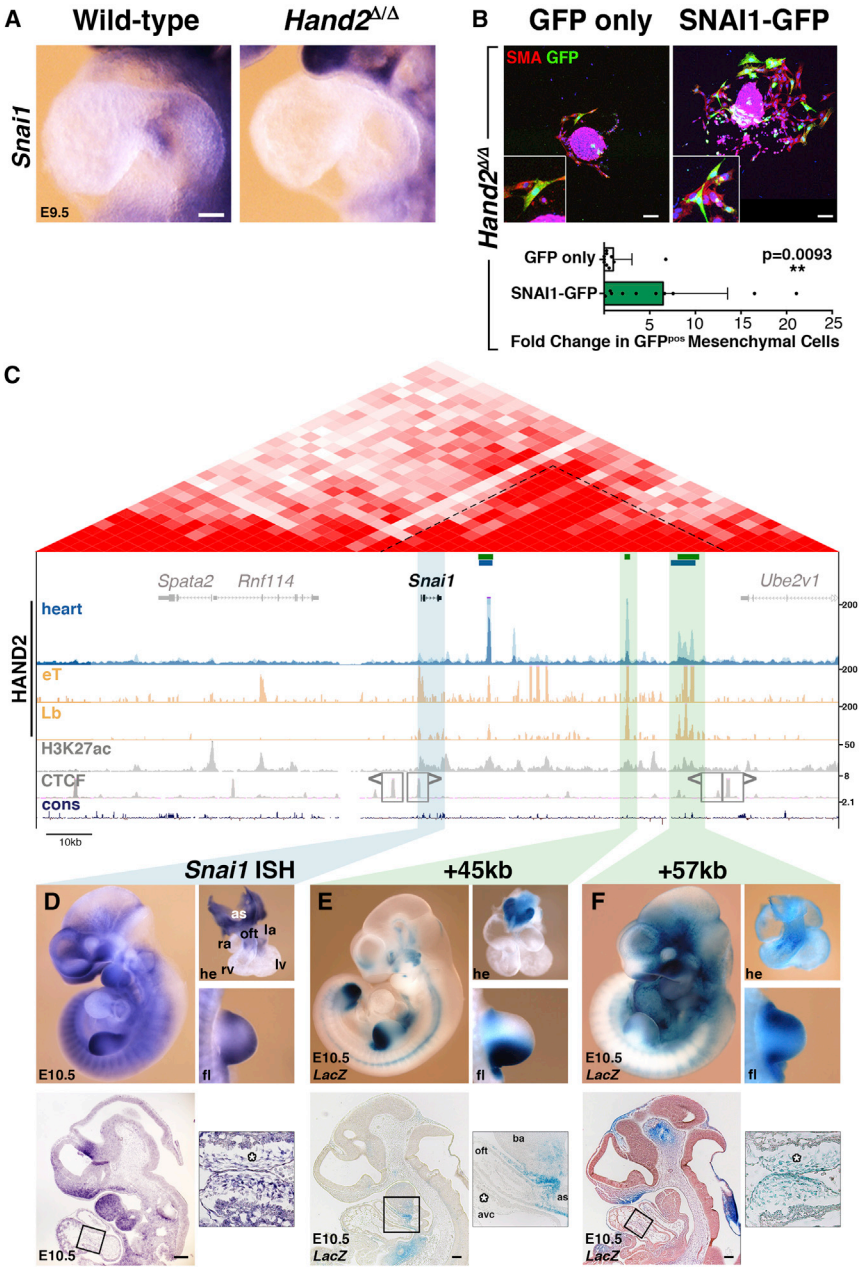

Figure 6. Re-expression of *Snai1* in *Hand2*-Deficient AVC Explants Partially Restores Mesenchymal Cell Migration and Regulation of *Snai1* Expression by Enhancers Enriched in HAND2 Chromatin Complexes

(A) *Snai1* expression is lost from the endocardium of *Hand2*-deficient hearts.

(B) Upper panels: *Hand2*-deficient AVC explants were infected either with GFP (control) or SNAI1-GFP adenovirus to re-express SNAI1. Samples were analyzed 72 hr after infection. All infected cells that migrated into the matrix are marked by GFP expression (green). Smooth muscle actin (SMA, red) was detected to reveal cellular morphology. Lower panel: quantitation of cell migration in *Hand2*-deficient AVC explants. The mean ± SD and all individual data points are shown. The observed increase in mesenchymal cells in SNAI1-GFP infected explants is significant ($p = 0.0093$, Mann-Whitney test). Scale bars, 100 μm.

(C) Scheme of the mouse *Snai1* TAD (red, HiC-data). The HAND2 ChIP-seq profiles in the heart (this study), *Hand2*-expressing tissues (eT) and limb buds (Lb) (Osterwalder et al., 2014) are shown below together with the H3K27ac profile in developing hearts (E11.5, Nord et al., 2013). The *Snai1* TAD boundaries are marked by CTCF-binding regions in opposite orientation (Gómez-Marín et al., 2015). Green bars indicate the HAND2 target CRMs located +14kb, +45kb, and +57kb that were analyzed by *LacZ* reporter assays in transgenic founder embryos.

(D) *Snai1* transcript distribution in wild-type mouse embryos (E10.5).

(E) A representative transgenic founder embryo (E10.5) shows the activity of *LacZ* reporter construct encoding the +45kb CRM. (F) A representative transgenic founder embryo (E10.5) shows the activity of *LacZ* reporter construct encoding the +57kb CRM. The upper panels in (E) and (F) depict whole embryos, dissected hearts, and forelimb buds. The lower panels show sagittal sections at the level of the heart. The boxed areas indicate the enlargements shown in the right panels.

Asterisks, AVC cardiac cushion mesenchyme; as, aortic sac; avc, atrioventricular canal; ba, branchial arch; la, left atria; lv, left ventricle; oft, outflow tract; ra, right atria; rv, right ventricle. Scale bars, 200 μm. See also Figures S5 and S6.

AVC explants with hyaluronic acid restores mesenchymal cell migration. In contrast, culturing *Hand2*-deficient AVC explants in hyaluronic acid does not suffice to restore migration (data not shown). This is in line with the fact that the genetic inactivation of *Hand2* affects the expression of multiple genes required for AVC cushion development (Figures 4 and S4).

HAND2 Regulates the Transcription of *Snai1*, a Key Regulator of the EMT and Mesenchymal Cell Migration in the AVC

The transcriptome combined with ChIP-seq/qPCR analysis (Figures 4D and 4E) and WISH (Figure 6A) establishes *Snai1* as a direct transcriptional target of HAND2. As *Snai1* is a EMT key regulator (Nieto, 2011), its loss from the mutant AVC (Figure 6A) is likely causally linked to the observed cardiac cushion agenesis (Figure 2). To test this experimentally, *Hand2*-deficient AVC explants were infected either with adenovirus producing both SNAI1 and GFP proteins (SNAI1-GFP) or control GFP virus (GFP only; Figure 6B; Tao et al., 2011). Quantitative analysis shows that infection of *Hand2*-deficient AVC explants with SNAI1-producing virus induces migration of a significantly larger fraction of GFP-positive mesenchymal cells into the collagen matrix than GFP alone (Figure 6B, $p = 0.0093$ Mann-Whitney test; see Figure S5C for wild-type controls).

This partial restoration of mesenchymal cell migration reveals the functional importance of the HAND2-*Snai1* interactions for the EMT during cardiac cushion formation. Therefore, we analyzed the potential enhancer activities of the three HAND2-interacting CRMs located in the *Snai1* TAD (Figures 6C and S6A). Our previous analysis has shown that these three candidate CRMs are also enriched in HAND2 chromatin complexes isolated from mouse limb buds (Osterwalder et al., 2014) and overlap regions of active chromatins in embryonic hearts (H3K27ac profile in Figure 6C). Their transcription enhancing potential was assessed in transgenic mouse founder embryos using *LacZ* reporter constructs (Figures 6E and 6F). In particular, *LacZ* activity reminiscent of *Snai1* expression (Figure 6D) was detected for reporters encoding the CRMs located +45kb and +57kb downstream of the *Snai1* transcription start site (Figures 6E and 6F). In contrast, no *LacZ* activity was detected using the *Snai1* +14kb genomic region, whose sequence is not well conserved in mammals (data not shown). The *Snai1* +45kb CRM is active in cells located between the OFT and aortic sac (n = 7/10), the posterior (n = 10/10) and anterior (n = 3/10) limb bud mesenchyme, and branchial arches and cranial mesenchyme (n = 5/10, Figure 6E). Most relevant with respect to the AVC, the *Snai1* +57kb CRM is active in the cardiac cushion mesenchyme of the AVC and OFT (n = 7/9, Figure 6F) and in most other embryonic tissues expressing *Snai1* (Figure 6D). Together, the activities of these two HAND2-interacting CRMs recapitulate most of the *Snai1* expression pattern in mouse embryos (Figures 6D and S6B–S6D). Indeed, in *Hand2*-deficient embryos, *Snai1* expression is not only lost from the AVC (Figure 6A), but also significantly reduced in the second branchial arch and forelimb bud mesenchyme (Figure S6E).

DISCUSSION

We show that HAND2 chromatin complexes interact with genomic regions such as enhancers located in the *cis*-regulatory landscapes of genes functioning in heart morphogenesis. Previous molecular analysis showed that the altered expression of many of these genes correlates well with the defects in right ventricle and OFT morphogenesis observed in *Hand2*-deficient mouse embryos (Cohen et al., 2012; Tsuchihashi et al., 2011; Zhao et al., 2008). We provide evidence that about half of all previously known genes with altered expression are direct transcriptional targets of HAND2. In addition, our ChIP-seq analysis reveals that a significant fraction of the genomic regions enriched in HAND2 chromatin complexes are also bound by GATA4 complexes (He et al., 2014). This is interesting in light of previous studies, which showed that HAND2 and GATA4 form transcriptional complexes regulating gene expression in developing hearts (Dai et al., 2002). In addition, it has been shown that AVC enhancers are repressed in the atrial and ventricular myocardium by complexes containing GATA4, HEY1, and/or HEY2 transcriptional repressors (Firulli et al., 2000; Stefanovic et al., 2014). These three repressors plus RUNX2 and TWIST1 are all able to form heterodimers with HAND2 (Firulli et al., 2005; Funato et al., 2009). As the expression of many HAND2 target genes is upregulated in *Hand2*-deficient AVCs (this study), HAND2-mediated transcriptional repression is likely functionally relevant to normal AVC development. For example, the HAND2 target *Hhex* is ectopically expressed in the AVC of *Hand2*-deficient embryos. Indeed, genetic inactivation of *Hhex* increases the number of mesenchymal cells in AVC cardiac cushions and causes valve dysplasia (Hallaq et al., 2004).

One key finding of our analysis is that constitutive inactivation of *Hand2* disrupts the EMT underlying cardiac cushion formation in the AVC. This disruption of AVC morphogenesis contrasts with the phenotypes resulting from specific inactivation of *Hand2* in either the endocardium or mesenchyme. Neither inactivation disrupts AVC cardiac cushion formation but specifically alters the AVC-derived tricuspid valves (tricuspid atresia; VanDusen et al., 2014a, 2014b). This discrepancy is a likely consequence of different *Hand2* inactivation kinetics. As genetic inactivation of *Hand2* in SHF progenitors also alters AVC development, we cannot formally exclude that recruitment of progenitors to the AVC is compromised in *Hand2*-deficient embryos (Tsuchihashi et al., 2011), even though the expression of early markers for AVC morphogenesis remains normal (this study).

However, our analysis shows that most genes with known functions in the EMT underlying AVC cardiac cushion formation are direct transcriptional targets of HAND2. Together with the cellular analysis, these results point to specific disruption of the EMT rather than a general arrest of AVC development and suggest that HAND2 is a very upstream regulator of AVC cardiac cushion morphogenesis. In agreement, re-expression of the HAND2 target *Snai1* in *Hand2*-deficient AVCs explants only partially restores mesenchymal cell migration, which indicates that other HAND2 target DEGs have essential functions in the EMT and/or mesenchymal cell migration during cardiac cushion development. Ingenuity pathway analysis of HAND2 target genes shows that HAND2 enhances the expression of genes such as *Msx1* and *Hnrnapab*, which, in turn, reinforce the expression of the HAND2 targets *Has2*, *Twist1*, and *Snai1* (Figure 7). This type of dual transcriptional reinforcement likely increases the robustness of the expression of HAND2 target genes with key functions in AVC morphogenesis. In fact, it is reminiscent of the dual transcriptional reinforcement seen for key genes during limb bud development. In early limb buds, HAND2 reinforces the expression of the *Shh* morphogen by directly regulating its transcription and indirectly via upregulating E26 transformation-specific (ETS) transcription factors, which also positively regulate *Shh* expression (Osterwalder et al., 2014).

Remarkably, this study identifies HAND2 as key regulator of most genes with known functions in EMT processes and cardiac cushion formation in the developing AVC including *Snai1* (Garside et al., 2013). We also provide evidence that HAND2 directly regulates *Snai1* transcription in other embryonic tissues. The notion that the direct transcriptional regulation of *Snai1* by HAND2 maybe of more general importance is supported by genetic analysis as *Hand2* and *Snai1* are both essential for the EMT of epicardial cells and morphogenesis of craniofacial structures such as the palate (Barnes et al., 2011; Murray et al., 2007; Tao et al., 2013; Xiong et al., 2009). In summary, our study identifies the HAND2 target GRN that controls the initiation of

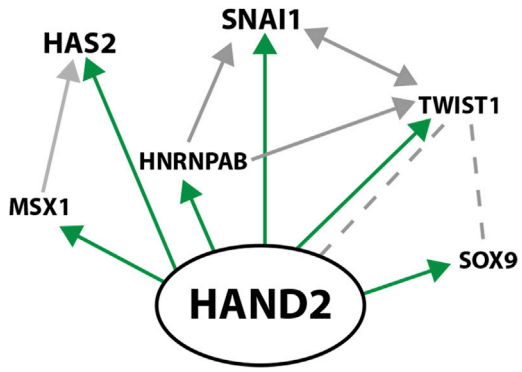

Figure 7. Scheme Depicting the Interactions among Positively Regulated HAND2 Targets Genes

The HAND2 GRN was constructed using Ingenuity pathway analysis in combination with manual annotation (Chen et al., 2008). Arrows indicate transcriptional upregulation and direct upregulation by HAND2 transcriptional complexes is indicated in green. Broken gray lines direct protein-protein interactions. This graph represents the simplest possible scheme to illustrate the relevant direct interactions.

cardiac valve formation and provides evidence for its general role in regulating the expression of *Snai1* during mouse embryogenesis. Last but not least, the identification of HAND2 as key regulator of AVC cardiac cushion morphogenesis may have important implications for regenerative medicine (see, e.g., review by Levine et al., 2015).

EXPERIMENTAL PROCEDURES

Ethics Statement, Mouse Strains, and Embryos

All experiments conducted with mice and embryos of both sexes at the developmental ages indicated (see Results and below) were performed in strict accordance with Swiss law. All animal studies were evaluated and approved by the Regional Commission on Animal Experimentation (license 1951). The 3Rs were taken into account in designing the animal studies. The procedures for generating transgenic mice at the Lawrence Berkeley National Laboratory (LBNL) were reviewed and approved by the LBNL Animal Welfare and Research Committee. The *Hand2*$^{\Delta}$ and *Hand2*^{3xF} alleles (Galli et al., 2010; Osterwalder et al., 2014) were outbred into an NMRI background as this prolongs survival of *Hand2*-deficient embryos in comparison to the previously used 129SvJ/C57BL6 background.

ChIP-Seq Analysis

To obtain sufficient material for ChIP-seq analysis, about 600 hearts had to be dissected from *Hand2*$^{3xF/3xF}$ mouse embryos at E10.5. After collection, these were split in two batches and processed as completely independent biological replicates for ChIP-seq analysis using the M2 anti-FLAG antibody (F1804; Sigma; (Osterwalder et al., 2014). Library construction and sequencing were performed by the Genome Technology Access Center using an Illumina HiSeq 2500 system. More details are included in the Supplemental Experimental Procedures.

Transcriptome Analysis

AVCs dissected from wild-type and *Hand2*$^{\Delta/\Delta}$ mutant embryos at E9.0–9.25 were flash frozen in RLT buffer (QIAGEN). Four AVCs were pooled per replicate, keeping the same gender ratio for all replicates (AVCs of two male and female embryos). RNA was extracted using the QIAGEN RNeasy mini kit. The quality of total RNA (30–60 ng) was analyzed using the Agilent 2100 Bioanalyzer, and both wild-type and mutant samples had an RNA integrity number (RIN) of 8.8–9.6. Libraries were prepared using the Clontech SMARTer kit and sequenced on a HiSeq3000 using a single-read 50 cycle protocol. More details on the computational analysis are provided in the Supplemental Experimental Procedures.

AVC Explant Cultures

AVC explant cultures were set on matrixes of rat-tail collagen type I (Luna-Zurita et al., 2010, see Supplemental Information for more details). Only wild-type and mutant AVC explants that were still beating, i.e., alive after 72 hr in culture were analyzed. Supplementation with hyaluronic acid (HA): both the collagen matrix and serum-free culture medium were supplemented with 0.75 mg/mL HA (Camenisch et al., 2000). Adenoviral infections: the titers of the SNAI1-GFP or GFP adenoviruses (Tao et al., 2011 and Vector Biolabs) were determined in mitomycin-treated mouse embryonic fibroblasts and adjusted such that equal numbers of active virus particles were used. Following attachment to the matrix, mutant and wild-type AVC explants were incubated with 6×10^6 plaque-forming units (PFUs) of either SNAI1-GFP or GFP virus for 12 hr in serum-free medium. Then, the AVC explants were cultured for 60 hr in fresh serum-free medium. After fixation in 4% paraformaldehyde (PFA) (30-min room temperature), antigens were detected using anti-SMA-Cy3 antibodies (1:250, Sigma) and Phalloidin-Alexa 488 (1:250, Life Technologies) and nuclei counterstained with Hoechst-33258 and analyzed using a Leica SP5 confocal microscope. The analysis of wild-type controls shows that GFP-virus tends to infect AVC cells more efficiently than SNAI1-GFP virus (Figure S5C). Therefore, the restoration of cell migration following infection of mutant AVCs with SNAI1-GFP virus is rather underestimated (Figure 6B).

Statistical Analysis

ChIP-seq

Following initial alignment of sequences, the genome-wide pattern of binding of HAND2 was determined using MACS (version 1.4.2) with a p value threshold of 1e-5.

ChIP-qPCR

Mean ± SD were calculated using the Prism (GraphPad Software) Student-t test.

Transcriptome

Following initial sequence alignment, *edgeR* was used to normalize the datasets (trimmed mean of M-values [TMM] normalization) and to identify the differentially expressed genes (DEGs). Only genes expressed in all samples were considered (reads per million [RPM] ≥ 1). DEGs are defined as genes with a q value ≤ 0.05 and a linear fold change ≥ 1.5.

AVC Explant Cultures

The Mann-Whitney test was used to determine significant differences in numbers of migrating mesenchymal cells. More details on statistical validation of the ChIP-seq and transcriptome analyses are included in the Supplemental Experimental Procedures.

Histology and Immunofluorescence Analysis

Embryos were collected and fixed overnight in 4% PFA at 4°C and embedded in paraffin wax. Standard protocols were used for histological staining (H&E; Alcian blue) of 7-μm paraffin sections. Minimally three biological replicates were analyzed for each stage, genotype, and antigen shown. Antibodies are listed the Supplemental Experimental Procedures.

Generation and Analysis of *LacZ* Transgenic Founder Embryos

Genomic regions were amplified by PCR from mouse genomic DNA (*Snai1* +45kb, *Snai1* +14kb) or recovered as restriction fragment (*Snai1* +57kb, BAC clone RP23-193B17) and cloned into the *Hsp68*-promoter-*LacZ* reporter vector (Osterwalder et al., 2014). Transgenic founder embryos were generated by pronuclear injection and analyzed by *LacZ* staining, and transgenic embryos were identified by genotyping.

ACCESSION NUMBERS

The accession numbers for the primary ChIP-seq and transcriptome datasets reported in this paper are GEO: GSE73368 and GSE94246, respectively.

SUPPLEMENTAL INFORMATION

Supplemental Information includes Supplemental Experimental Procedures, six figures, and six tables and can be found with this article online at http://dx.doi.org/10.1016/j.celrep.2017.05.004.

AUTHOR CONTRIBUTIONS

F.L. performed the ChIP-seq and follow-up functional analysis, A.G. performed the transcriptome and WISH analysis for revision, J.G. participated in different aspects of the experimental studies, and I.B. performed the bioinformatics analysis. M.O. was involved in initiating this study, J.L. generated the SNAI1-GFP virus, J.A.A. generated the *LacZ* reporters, and A.V. provided the resources for the transgenic and bioinformatics analysis. The experimental study design was done and the manuscript written by F.L., J.L.-R., A.Z., and R.Z. with input from all authors.

ACKNOWLEDGMENTS

The Genome Technology Access Center (Department of Genetics at Washington University School of Medicine) is acknowledged for deep sequencing, and R. Ivanek (DBM Bioinformatics Core) performed the bioinformatics analysis of the ChIP-seq datasets. All calculations were performed using the sciCORE (https://scicore.unibas.ch/) scientific computing core facility at University of Basel. We thank D. Speziale for technical assistance, A. Offinger's team for excellent animal care, and P. Lorentz (DBM Bio-Optics Core Facility) for imaging support. V. Afzal, B. Mannion, and I. Plajzer-Frick provided assistance with transgenics, and L. Bazzani provided the GFP adenovirus preparations. T. Papoutsi, C. Rolando, and O. Pertz are acknowledged for advice on AVC explants and infections. We are grateful to V. Christoffels for helpful input and anonymous reviewers for critical input that resulted in a significantly improved study. This research was mostly supported by SNF grants 31003A_146248 and 310030B_166685 to A.Z. and R.Z. and by funds from the University of Basel. The stay of M.O. in the group of A.V. was supported by an SNSF early mobility postdoctoral fellowship. I.B., J.A., and A.V. were supported by NIH grants R24HL123879, UM1HL098166, R01HG003988, and U54HG006997, and research at LBNL was performed under Department of Energy Contract DE-AC02-05CH11231 to University of California. J.L. was supported by NIH/NHLBI grant 1R01HL127033.

Received: May 20, 2016
Revised: March 20, 2017
Accepted: April 28, 2017
Published: May 23, 2017

REFERENCES

Akiyama, H., Chaboissier, M.C., Behringer, R.R., Rowitch, D.H., Schedl, A., Epstein, J.A., and de Crombrugghe, B. (2004). Essential role of Sox9 in the pathway that controls formation of cardiac valves and septa. Proc. Natl. Acad. Sci. USA *101*, 6502–6507.

Barnes, R.M., Firulli, B.A., VanDusen, N.J., Morikawa, Y., Conway, S.J., Cserjesi, P., Vincentz, J.W., and Firulli, A.B. (2011). Hand2 loss-of-function in Hand1-expressing cells reveals distinct roles in epicardial and coronary vessel development. Circ. Res. *108*, 940–949.

Bruneau, B.G. (2008). The developmental genetics of congenital heart disease. Nature *451*, 943–948.

Camenisch, T.D., Spicer, A.P., Brehm-Gibson, T., Biesterfeldt, J., Augustine, M.L., Calabro, A., Jr., Kubalak, S., Klewer, S.E., and McDonald, J.A. (2000). Disruption of hyaluronan synthase-2 abrogates normal cardiac morphogenesis and hyaluronan-mediated transformation of epithelium to mesenchyme. J. Clin. Invest. *106*, 349–360.

Chen, Y.H., Ishii, M., Sucov, H.M., and Maxson, R.E., Jr. (2008). Msx1 and Msx2 are required for endothelial-mesenchymal transformation of the atrioventricular cushions and patterning of the atrioventricular myocardium. BMC Dev. Biol. *8*, 75.

Christoffels, V.M., Smits, G.J., Kispert, A., and Moorman, A.F. (2010). Development of the pacemaker tissues of the heart. Circ. Res. *106*, 240–254.

Cohen, E.D., Miller, M.F., Wang, Z., Moon, R.T., and Morrisey, E.E. (2012). Wnt5a and Wnt11 are essential for second heart field progenitor development. Development *139*, 1931–1940.

Dai, Y.S., and Cserjesi, P. (2002). The basic helix-loop-helix factor, HAND2, functions as a transcriptional activator by binding to E-boxes as a heterodimer. J. Biol. Chem. *277*, 12604–12612.

Dai, Y.S., Cserjesi, P., Markham, B.E., and Molkentin, J.D. (2002). The transcription factors GATA4 and dHAND physically interact to synergistically activate cardiac gene expression through a p300-dependent mechanism. J. Biol. Chem. *277*, 24390–24398.

Dixon, J.R., Selvaraj, S., Yue, F., Kim, A., Li, Y., Shen, Y., Hu, M., Liu, J.S., and Ren, B. (2012). Topological domains in mammalian genomes identified by analysis of chromatin interactions. Nature *485*, 376–380.

Firulli, B.A., Hadzic, D.B., McDaid, J.R., and Firulli, A.B. (2000). The basic helix-loop-helix transcription factors dHAND and eHAND exhibit dimerization characteristics that suggest complex regulation of function. J. Biol. Chem. *275*, 33567–33573.

Firulli, B.A., Krawchuk, D., Centonze, V.E., Vargesson, N., Virshup, D.M., Conway, S.J., Cserjesi, P., Laufer, E., and Firulli, A.B. (2005). Altered Twist1 and Hand2 dimerization is associated with Saethre-Chotzen syndrome and limb abnormalities. Nat. Genet. *37*, 373–381.

Funato, N., Chapman, S.L., McKee, M.D., Funato, H., Morris, J.A., Shelton, J.M., Richardson, J.A., and Yanagisawa, H. (2009). Hand2 controls osteoblast differentiation in the branchial arch by inhibiting DNA binding of Runx2. Development *136*, 615–625.

Galli, A., Robay, D., Osterwalder, M., Bao, X., Bénazet, J.D., Tariq, M., Paro, R., Mackem, S., and Zeller, R. (2010). Distinct roles of Hand2 in initiating polarity and posterior Shh expression during the onset of mouse limb bud development. PLoS Genet. *6*, e1000901.

Garside, V.C., Chang, A.C., Karsan, A., and Hoodless, P.A. (2013). Co-ordinating Notch, BMP, and TGF-β signaling during heart valve development. Cell. Mol. Life Sci. *70*, 2899–2917.

Gómez-Marín, C., Tena, J.J., Acemel, R.D., López-Mayorga, M., Naranjo, S., de la Calle-Mustienes, E., Maeso, I., Beccari, L., Aneas, I., Vielmas, E., et al. (2015). Evolutionary comparison reveals that diverging CTCF sites are signatures of ancestral topological associating domains borders. Proc. Natl. Acad. Sci. USA *112*, 7542–7547.

Greulich, F., Rudat, C., and Kispert, A. (2011). Mechanisms of T-box gene function in the developing heart. Cardiovasc. Res. *91*, 212–222.

Hallaq, H., Pinter, E., Enciso, J., McGrath, J., Zeiss, C., Brueckner, M., Madri, J., Jacobs, H.C., Wilson, C.M., Vasavada, H., et al. (2004). A null mutation of Hhex results in abnormal cardiac development, defective vasculogenesis and elevated Vegfa levels. Development *131*, 5197–5209.

He, A., Gu, F., Hu, Y., Ma, Q., Ye, L.Y., Akiyama, J.A., Visel, A., Pennacchio, L.A., and Pu, W.T. (2014). Dynamic GATA4 enhancers shape the chromatin landscape central to heart development and disease. Nat. Commun. *5*, 4907.

Heinz, S., Benner, C., Spann, N., Bertolino, E., Lin, Y.C., Laslo, P., Cheng, J.X., Murre, C., Singh, H., and Glass, C.K. (2010). Simple combinations of lineage-determining transcription factors prime cis-regulatory elements required for macrophage and B cell identities. Mol. Cell *38*, 576–589.

Holler, K.L., Hendershot, T.J., Troy, S.E., Vincentz, J.W., Firulli, A.B., and Howard, M.J. (2010). Targeted deletion of Hand2 in cardiac neural crest-derived cells influences cardiac gene expression and outflow tract development. Dev. Biol. *341*, 291–304.

Kelly, R.G. (2012). The second heart field. Curr. Top. Dev. Biol. *100*, 33–65.

Levine, R.A., Hagége, A.A., Judge, D.P., Padala, M., Dal-Bianco, J.P., Aikawa, E., Beaudoin, J., Bischoff, J., Bouatia-Naji, N., Bruneval, P., et al.; Leducq Mitral Transatlantic Network (2015). Mitral valve disease–morphology and mechanisms. Nat. Rev. Cardiol. *12*, 689–710.

Lin, C.J., Lin, C.Y., Chen, C.H., Zhou, B., and Chang, C.P. (2012). Partitioning the heart: mechanisms of cardiac septation and valve development. Development *139*, 3277–3299.

Liu, N., Barbosa, A.C., Chapman, S.L., Bezprozvannaya, S., Qi, X., Richardson, J.A., Yanagisawa, H., and Olson, E.N. (2009). DNA binding-dependent and -independent functions of the Hand2 transcription factor during mouse embryogenesis. Development *136*, 933–942.

Luna-Zurita, L., Prados, B., Grego-Bessa, J., Luxán, G., del Monte, G., Benguría, A., Adams, R.H., Pérez-Pomares, J.M., and de la Pompa, J.L. (2010). Integration of a Notch-dependent mesenchymal gene program and Bmp2-driven cell invasiveness regulates murine cardiac valve formation. J. Clin. Invest. *120*, 3493–3507.

Ma, L., Lu, M.F., Schwartz, R.J., and Martin, J.F. (2005). Bmp2 is essential for cardiac cushion epithelial-mesenchymal transition and myocardial patterning. Development *132*, 5601–5611.

MacGrogan, D., Luxán, G., Driessen-Mol, A., Bouten, C., Baaijens, F., and de la Pompa, J.L. (2014). How to make a heart valve: from embryonic development to bioengineering of living valve substitutes. Cold Spring Harb. Perspect. Med. *4*, a013912.

McLean, C.Y., Bristor, D., Hiller, M., Clarke, S.L., Schaar, B.T., Lowe, C.B., Wenger, A.M., and Bejerano, G. (2010). GREAT improves functional interpretation of cis-regulatory regions. Nat. Biotechnol. *28*, 495–501.

Murray, S.A., Oram, K.F., and Gridley, T. (2007). Multiple functions of Snail family genes during palate development in mice. Development *134*, 1789–1797.

Niessen, K., Fu, Y., Chang, L., Hoodless, P.A., McFadden, D., and Karsan, A. (2008). Slug is a direct Notch target required for initiation of cardiac cushion cellularization. J. Cell Biol. *182*, 315–325.

Nieto, M.A. (2011). The ins and outs of the epithelial to mesenchymal transition in health and disease. Annu. Rev. Cell Dev. Biol. *27*, 347–376.

Nord, A.S., Blow, M.J., Attanasio, C., Akiyama, J.A., Holt, A., Hosseini, R., Phouanenavong, S., Plajzer-Frick, I., Shoukry, M., Afzal, V., et al. (2013). Rapid and pervasive changes in genome-wide enhancer usage during mammalian development. Cell *155*, 1521–1531.

Osterwalder, M., Speziale, D., Shoukry, M., Mohan, R., Ivanek, R., Kohler, M., Beisel, C., Wen, X., Scales, S.J., Christoffels, V.M., et al. (2014). HAND2 targets define a network of transcriptional regulators that compartmentalize the early limb bud mesenchyme. Dev. Cell *31*, 345–357.

Shen, L., Li, X.F., Shen, A.D., Wang, Q., Liu, C.X., Guo, Y.J., Song, Z.J., and Li, Z.Z. (2010). Transcription factor HAND2 mutations in sporadic Chinese patients with congenital heart disease. Chin. Med. J. (Engl.) *123*, 1623–1627.

Srivastava, D., Thomas, T., Lin, Q., Kirby, M.L., Brown, D., and Olson, E.N. (1997). Regulation of cardiac mesodermal and neural crest development by the bHLH transcription factor, dHAND. Nat. Genet. *16*, 154–160.

Stefanovic, S., and Christoffels, V.M. (2015). GATA-dependent transcriptional and epigenetic control of cardiac lineage specification and differentiation. Cell. Mol. Life Sci. *72*, 3871–3881.

Stefanovic, S., Barnett, P., van Duijvenboden, K., Weber, D., Gessler, M., and Christoffels, V.M. (2014). GATA-dependent regulatory switches establish atrioventricular canal specificity during heart development. Nat. Commun. *5*, 3680.

Sun, Y.M., Wang, J., Qiu, X.B., Yuan, F., Li, R.G., Xu, Y.J., Qu, X.K., Shi, H.Y., Hou, X.M., Huang, R.T., et al. (2016). A HAND2 loss-of-function mutation causes familial ventricular septal defect and pulmonary stenosis. G3 (Bethesda) *6*, 987–992.

Tao, G., Levay, A.K., Gridley, T., and Lincoln, J. (2011). Mmp15 is a direct target of Snai1 during endothelial to mesenchymal transformation and endocardial cushion development. Dev. Biol. *359*, 209–221.

Tao, G., Miller, L.J., and Lincoln, J. (2013). Snai1 is important for avian epicardial cell transformation and motility. Dev. Dyn. *242*, 699–708.

Timmerman, L.A., Grego-Bessa, J., Raya, A., Bertrán, E., Pérez-Pomares, J.M., Díez, J., Aranda, S., Palomo, S., McCormick, F., Izpisúa-Belmonte, J.C., and de la Pompa, J.L. (2004). Notch promotes epithelial-mesenchymal transition during cardiac development and oncogenic transformation. Genes Dev. *18*, 99–115.

Tsuchihashi, T., Maeda, J., Shin, C.H., Ivey, K.N., Black, B.L., Olson, E.N., Yamagishi, H., and Srivastava, D. (2011). Hand2 function in second heart field progenitors is essential for cardiogenesis. Dev. Biol. *351*, 62–69.

VanDusen, N.J., and Firulli, A.B. (2012). Twist factor regulation of non-cardiomyocyte cell lineages in the developing heart. Differentiation *84*, 79–88.

VanDusen, N.J., Casanovas, J., Vincentz, J.W., Firulli, B.A., Osterwalder, M., Lopez-Rios, J., Zeller, R., Zhou, B., Grego-Bessa, J., De La Pompa, J.L., et al. (2014a). Hand2 is an essential regulator for two Notch-dependent functions within the embryonic endocardium. Cell Rep. *9*, 2071–2083.

VanDusen, N.J., Vincentz, J.W., Firulli, B.A., Howard, M.J., Rubart, M., and Firulli, A.B. (2014b). Loss of Hand2 in a population of Periostin lineage cells results in pronounced bradycardia and neonatal death. Dev. Biol. *388*, 149–158.

Visel, A., Minovitsky, S., Dubchak, I., and Pennacchio, L.A. (2007). VISTA Enhancer Browser–a database of tissue-specific human enhancers. Nucleic Acids Res. *35*, D88–D92.

Wu, Z.Q., Rowe, R.G., Lim, K.C., Lin, Y., Willis, A., Tang, Y., Li, X.Y., Nor, J.E., Maillard, I., and Weiss, S.J. (2014). A Snail1/Notch1 signalling axis controls embryonic vascular development. Nat. Commun. *5*, 3998.

Xiong, W., He, F., Morikawa, Y., Yu, X., Zhang, Z., Lan, Y., Jiang, R., Cserjesi, P., and Chen, Y. (2009). Hand2 is required in the epithelium for palatogenesis in mice. Dev. Biol. *330*, 131–141.

Zhang, Y., Liu, T., Meyer, C.A., Eeckhoute, J., Johnson, D.S., Bernstein, B.E., Nusbaum, C., Myers, R.M., Brown, M., Li, W., and Liu, X.S. (2008). Model-based analysis of ChIP-Seq (MACS). Genome Biol. *9*, R137.

Zhao, R., Watt, A.J., Battle, M.A., Li, J., Bondow, B.J., and Duncan, S.A. (2008). Loss of both GATA4 and GATA6 blocks cardiac myocyte differentiation and results in acardia in mice. Dev. Biol. *317*, 614–619.